Small-Angle X-ray Scattering and NMR Studies of the Conformation of the PDZ Region of SAP97 and Its Interactions with Kir2.1†

Benjamin T. Goult,[‡,§] Jonathan D. Rapley,[§,∥,⊥] Caroline Dart,[#] Ashraf Kitmitto,[@] J. Günter Grossmann,[+] Mark L. Leyland,[‡] and Lu-Yun Lian*[,#]

Department of Biochemistry, University of Leicester, Leicester LE1 9HN, United Kingdom, Faculty of Life Sciences, The University of Manchester, Manchester M60 1QD, United Kingdom, School of Biological Sciences, Biosciences Building, Crown Street, University of Liverpool, Liverpool L69 7ZB, United Kingdom, School of Medicine, Cardiovascular and Endocrine Sciences, The University of Manchester, Manchester M13 9PT, United Kingdom, and Molecular Biophysics Group, Science and Technology Facilities Council Daresbury Laboratory, Daresbury Science and Innovation Campus, Warrington WA4 4AD, United Kingdom

Received June 26, 2007; Revised Manuscript Received September 6, 2007

ABSTRACT: The functional localization of potassium inward rectifiers is regulated by SAP97, a PDZ membrane-associated guanylate kinase protein. We describe here an investigation of the conformation of the PDZ domain region of SAP97 PDZ1−3. The NMR and SAXS data reveal conformational dynamics. The NMR data show minimal interdomain contacts, with the U3 linker region between PDZ2 and PDZ3 being largely unstructured. Shape analysis of the SAXS profiles revealed a dumbbell for the PDZ12 double domain. An overall elongated, asymmetric shape comprised of two to three distinct components characterizes the triple domain PDZ1−3. In addition, rigid body modeling shows that the representative average shape does not provide the full picture and that the data for the triple domain are consistent with large variations, suggesting significant conformational flexibility. However, the dynamics appears to be restricted as PDZ3 is located essentially within ∼40 Å from PDZ12. We also show that the Kir2.1 cytoplasmic domain interacts with all three PDZ domains but with a clear preference for PDZ2 even in the presence of the U3 region. We speculate that the restricted dynamics and preferential Kir2.1 binding to PDZ2 are features that enable SAP97 to function as a scaffold protein, allowing other proteins each to bind to the other two PDZ domains in sufficient proximity to yield productive channelosomes.

SAP97 is a member of the membrane-associated guanylate kinases (MAGUKs) superfamily of proteins that interacts with a range of other proteins such as the ion channels, adhesion molecules, other cytoskeletal proteins, and subunits of glutamate receptors (*1*−*4*). Like other MAGUK proteins, SAP97 is a multidomain protein; it has an L27 N-terminal domain followed by three PSD-95/SAP90-DLG-ZO1 (PDZ)[1] domains, and a src homologue 3 (SH3) and guanylate kinase (GUK)-like domain at the C-terminus. In addition to the conserved protein domains, SAP97 has five unique regions, U1−U5, and an alternatively spliced I3 insertion region (Figure 1) (*5*, *6*). The conserved protein domains are sites of protein−protein interactions. Structures of the SAP97 L27 multimerization domain (*7*) and the single PDZ domains (PDZ1 (*8*), PDZ2 (*9*), and PDZ3 (*10*, *11*)) have been reported. In addition, the crystal structures of the SH3-GUK domain from the closely related PSD-95 have also been reported (*12*, *13*).

The PDZ domains of SAP97, like most PDZ domains, recognize the consensus C-terminal motif X-T/S-X-Φ-COOH, where Φ is a hydrophobic amino acid. The PDZ domain is comprised of six β-strands and two α-helices that fold into a six-stranded β-sandwich. The peptide ligands bind in an extended groove between β_B and α_B serving as an additional antiparallel β-strand within the PDZ domain. The GLGF motif or carboxylate-binding loop in the PDZ domain is located between βA and βB and creates a hydrophobic cavity to accommodate the hydrophobic carboxyl terminus residue of the partner protein. From the structures of PDZ-peptide complexes now available, the emerging picture is that amino acids beyond the four-residue X-T/S-X-Φ-COOH

† This work was supported by grants from the British Heart Foundation (PG/1999066 to L.-Y.L. and C.D.), PG/2000130 (M.L.L.), BS/97002 (A.K.), the Wellcome Trust (Grant 057806 to L.-Y.L.), and BBSRC (Research Studentship to J.D.R.).

* Corresponding author. E-mail: lu-yun.lian@liverpool.ac.uk; tel.: + (44) 151 7945 4458; fax: + (44) 151 795 4414.

‡ University of Leicester.

§ B.T.G. and J.D.R. contributed equally to this work.

∥ Faculty of Life Sciences, The University of Manchester.

⊥ Current address: Division of Immune Cell Biology and Division of Molecular Structure, MRC National Institute for Medical Research, The Ridgeway, Mill Hill, London NW7 1AA, United Kingdom.

University of Liverpool.

@ School of Medicine, Cardiovascular and Endocrine Sciences, The University of Manchester.

+ Science and Technology Facilities Council Daresbury Laboratory.

[1] Abbreviations: aa, amino acid; Kir, potasssium inward rectifier; KirNC, Kir residues 1-67-GG-189-428; HSQC, heteronuclear single quantum coherence; NOE, nuclear Overhauser effect; NOESY, NOE spectroscopy; PDZ, PSD-95/SAP90-DLG-ZO1; SAP97 PDZ1, residues 218−313; SAP97 PDZ2, residues 314−406, SAP97 PDZ3, residues 458−548; SAP97 U3 + PDZ3 + U4, residues 407−577, SAP97 PDZ12, residues 218−406; SAP97, PDZ1−3, residues 218−577; SAP97, synapse-associated protein-97; SAXS, small-angle X-ray scattering.

10.1021/bi701257z CCC: $37.00
Published on Web 11/16/2007

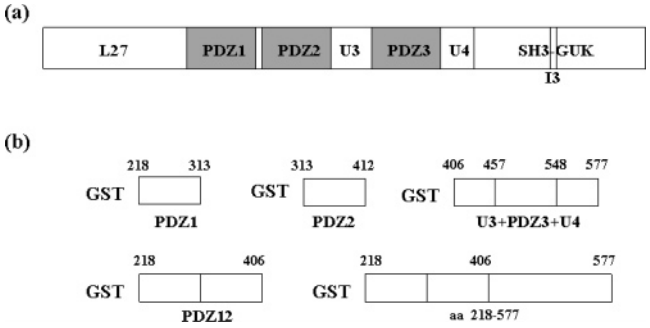

FIGURE 1: (a) Schematic diagram of the domain organization of rat SAP97 highlighting the position of the domains relevant in this study. (b) Schematic representation of the recombinant SAP97 proteins used in this study. The number system corresponds to the sequence of the full-length rat SAP97.

canonical PDZ recognition motif of the partner protein form additional contacts with the PDZ domain. These extra interactions account for the differences in specificities and affinities for different PDZ domains.

There are no high-resolution structures of full-length SAP97. Low-resolution negative-stain electron microscopy and single particle analysis of SAP97 show a mixture of conformations with about 65% appearing as extended rod-like monomeric particles and the remaining 35% as C-shaped/ring-like structures (*14*). Biochemical studies on the binding of SAP97 with other proteins imply the presence of intramolecular interactions between N and C regions of the full-length protein (*15*) and between SH3 and PDZ3 regions (*16*).

The inward rectifier family of potassium channels (Kir) is important for a wide variety of physiological functions such as regulation of the resting membrane potential, control of neuronal excitability and heart rate, and potassium homeostasis (*17*−*19*). The subcellular localization and surface density of Kir channels can be regulated through interactions with an intracellular scaffolding protein. Members of the classical strong inwardly rectifying Kir2 subfamily, Kir2.1, Kir2.2, and Kir2.3, contain a PDZ interaction motif at their C-termini. They have been shown to bind to MAGUKs, PSD-95/SAP90, SAP97/hDlg, and PSD-93/chapsyn 110 (*20*−*26*). Crystal structures of the tetrameric Kir2.1 and 3.1 cytoplasmic domains have been reported (*27*−*29*), although the conformations of the C-termini that contain the PDZ-binding motifs remain unknown in these crystal structures. A recent NMR study showed that the C-terminus tail of Kir2.1 (residues 372−428) is highly flexible and largely unstructured (*30*).

There are reports of specific interactions involving the PDZ region of SAP97: PDZ1 binds preferentially to NR2A of the NMDA receptor (*31*), PDZ2 to Kir2.1/2.3 (*24*), PDZ3 to TACE (*32*), PDZ1 and PDZ3 to SAPK3/p38γ (*33*), and the U3 region to caveolin-3 (*34*). One critical question about these interactions is whether all the PDZ domains in the aa 218−577 region are able to bind to the different target proteins at the same time. In the general field of MAGUK scaffold proteins, despite the roles of these proteins in bringing several proteins together to form receptosomes, and channelosomes, there have been few detailed structural investigations of how such complexes might form.

We report here an investigation of the structural aspects of the PDZ region (aa 218−577) of SAP97 (referred to as PDZ1−3 in the text for ease of reference) and its interactions with the tetrameric cytoplasmic domain of Kir2.1, which is comprised of the N (aa 1−67) domain fused to C (aa 189−428). The conformation of the PDZ region was determined using a combination of nuclear magnetic resonance (NMR) and small-angle X-ray scattering (SAXS). The NMR data of the complex shows Kir2.1 binding to all three PDZ domains with a preferential affinity for the second PDZ domain. We also show that the U3 region does not appear to undergo significant conformational change to allow Kir to bind PDZ2. The SAXS data reveal the presence of restricted conformational dynamics, with PDZ3 sampling a limited space and tethered to PDZ12. The mode of interactions described suggests the possibility that the other two PDZ domains are free to bind to other proteins to form a channelosome.

EXPERIMENTAL PROCEDURES

Expression Plasmids. Rat SAP97 PDZ constructs: PDZ domains from SAP97, PDZ1 (aa 218−313), PDZ2 (aa 314−406), U3 + PDZ3 + U4 (aa 407−577), PDZ12 (aa 218−406), and PDZ1−3 (aa 218−577) were PCR amplified from pEGFP-SAP97 (a generous gift from Dr. C. Garner, University of Birmingham). PCR products were gel-purified, A-tailed, and cloned into pGEM-T (Promega) before being subcloned and inserted between BamHI and EcoRI sites of the GST-fusion protein vector, pGEX-6P-1 (Amersham Biosciences). All inserts were verified by automated sequencing (PNACL Facility, University of Leicester). SAP97 PDZ2 in the plasmid construct pGEX-2TK was a generous gift from Dr. Ronald Javier (Baylor College of Medicine) (*35*). Mouse KirNC construct (1−67-GlyGly-189−428) in the pET15b vector was a gift from Steve Prince (Faculty of Life Sciences, The University of Manchester). Construction of the C275S mutant in PDZ1−3 was performed using the QuikChange mutagenesis kit (Strategene). Incorporation of the mutation was verified by sequencing the entire PDZ1−3 coding region.

Isotope Labeling of Proteins. Isotope-labeled samples were prepared by culturing BL21 (DE3) cells in isotope-labeled 2M9 based minimal media with ^{15}N-labeled ammonium chloride and ^{13}C-labeled glucose as the sole nitrogen and carbon sources, respectively. For deuterated proteins, D_2O (99.99% deuterium) was used to prepare the media.

Expression and Purification of the PDZ Domains of SAP97. PGEX-6P constructs of PDZ1, U3 + PDZ3 + U4, PDZ12, and PDZ1−3 and a pGEX-6T construct of PDZ2 were expressed in *Escherichia coli* BL21 (DE3) cells. Unlabeled proteins were produced at 37 °C in Luria broth; cells were grown to induction density (0.7), induced with 1 mM IPTG, and incubated for a further 3 h before harvesting. For the production of ^{15}N/^{2}H proteins, cells were grown to induction density (0.7) in unlabeled minimal media; the culture was harvested and resuspended in a quarter of the original volume of ^{15}N/D_2O minimal media. Following induction by IPTG, the cells were grown for a further 3 h in labeled media. Harvested cells were resuspended in phosphate buffered saline (PBS) pH 7.3 containing the Complete Protease Inhibitor Cocktail EDTA-Free Tablets (Roche Molecular Biochemicals). Cells were lysed by a French press; soluble and insoluble proteins were separated by centrifuga-

tion at 20 000 rpm for 20 min. Filtered supernatant was loaded onto Glutathione Sepharose 4B (Amersham Biosciences) columns at room temperature and washed with 10 volumes of PBS. Resin loaded with protein expressed in pGEX-6T (SAP 97 PDZ2) was resuspended in PBS. Following the addition of 50 units of thrombin (Amersham Biosciences), the resin was incubated with shaking at 4 °C for 16 h. In the case of proteins expressed in pGEX-6P (PDZ1, PDZ12, and PDZ1−3), the protein loaded resins were resuspended in 50 mM Tris-HCL pH 7.0, 140 mM NaCl, 1 mM EDTA, and 1 mM DTT and incubated with 0.5 mg of Precision Protease per milliliter of the Glutathione Sepharose 4B resin at 4 °C with shaking for 16 h. Following proteolytic cleavage of the target protein from the GST, PDZ proteins were washed from the Sepharose resin using PBS for PDZ2 and 50 mM Tris-HCl pH 7.0, 140 mM NaCl, 1 mM EDTA, and 1 mM DTT for all other proteins. PDZ1 and PDZ2 were purified to homogeneity using a Superdex 75 column (Amersham Biosciences) equilibrated in 50 mM phosphate pH 7.5, 50 mM NaCl, 2 mM DTT, and 1 mM EDTA; the elution volume of both proteins from this column was consistent with a molecular weight of 10 kDa. PDZ12 was dialyzed into 50 mM phosphate pH 8.0, 2 mM DTT, and 1 mM EDTA and purified to homogeneity using a Resource Q column (Amersham Biosciences); the protein was eluted between 50 and 100 mM NaCl. The buffer for PDZ1−3 was exchanged to 25 mM acetate buffer, 1 mM EDTA, and 2 mM DTT and purified to homogeneity using a Resource S column (Amersham Biosciences). Purified proteins were identified by tryptic digest of gel bands containing the purified protein, and the resulting solution was subjected to matrix-assisted laser desorption ionization followed by time-of-flight mass spectrometry (MALDI-TOF). The predicted fragment sizes matched experimental values for all proteins.

Expression and Purification of KirNC. Cells transformed with a pET15b plasmid containing the insert were grown to induction point ($OD_{595} = 0.7$) at 37 °C, incubated on ice for 10 min, and induced with 1 mM IPTG. After 5 h incubation at 25 °C, the cells were lysed by a French press in phosphate buffer (pH 8) containing 0.5 M NaCl, 2 mM DTT, and Complete Protease Inhibitor Cocktail EDTA-Free tablets. The lysate was loaded to an Amersham His-Trap Ni affinity column and washed with 100 mM imidazole, and the protein eluted with 300 mM imidazole. Further purification by gel filtration in 50 mM phosphate pH 7.5, 50 mM NaCl, 2 mM DTT, and 1 mM EDTA using a Superdex 200 Column (Amersham) gave pure protein; the elution volume suggests that the protein was likely to be an octamer. Several other buffer conditions were explored in an attempt to produce a tetrameric form of the protein; none appeared to be considerably better than the phosphate buffer. The purified protein was confirmed to be KirNC by tryptic digest MALDI-TOF.

Fluorescence Spectroscopy. Fluorescence anisotropy data were collected at 25 °C on a Varian Cary Eclipse spectrofluorimeter using a 3 mL quartz cuvette. Excitation and emitted lights were polarized using a manual Varian polarizer. Peptide binding was determined using the N-terminal fluorescein-labeled peptide ^{418}EPRPLRRESEI^{428} (Peptide Protein Research Ltd.) at a concentration of 0.1 μM and varying the PDZ protein concentration from 0.10 to 500−650 μM in 50 mM phosphate buffer with 50 mM NaCl, 2 mM DTT, and 1 mM EDTA at pH 7.5. The data were analyzed by GraphPad Prism 5 software using a nonlinear least-squares fit for one- and two-site binding models.

Spin Labeling of SAP97. We used the C275S mutant for these studies. The required amount of the spin-labeled MTSL ((1-oxyl-2,2,5,5-tetramethyl-Δ^3-pyrroline-3-methyl)methanethiosulfonate) (Toronto Research Chemicals Inc.) was dissolved in acetonitrile and added to the protein solution to yield a final MTSL/protein ratio of 5:1. The reaction was performed at 4 °C under nitrogen for 16 h. Unreacted spin label was removed by centrifugation, followed by a PD10 gel filtration column (Amersham). The spin-labeled protein was concentrated to a final concentration of 0.4 mM using a 5 kDa MWCO Amicon concentrator. Determination of degree of spin labeling was achieved using the Ellman Assay. The spin-labeling reaction was shown to be efficient with 80−90% of free cysteines coupled after 16 h at 4 °C. EPR was used to confirm that the spin label was covalently attached and to establish the oxidation state of each of the NMR samples (oxidized or reduced). Reduction of the spin label was achieved by the addition of a 5-fold excess of ascorbate from a stock solution. The ^{15}N-HSQC spectrum of wild type PDZ1−3, its C275S mutant, and the reduced form of the cysteine-attached MTSL protein all gave nearly identical spectra, confirming that neither the serine to cysteine mutation nor the covalent attachment of a nitroxide group caused significant structural perturbation.

NMR Sample Preparation. The NMR samples were all between 0.5 and 1 mM. For resonance assignments, each of the individual PDZ domains was made up using a buffer solution containing 20 mM phosphate, 50 mM NaCl, 1 mM EDTA, and 1 mM NaN_3 in 90% H_2O/10% D_2O at pH 6.5.

PDZ samples for interactions were made up in 50 mM NaCl, 1 mM EDTA, and 1 mM NaN_3 in 90% H_2O/10% D_2O at pH 7.5. This was shown to be optimal for the stability of KirNC and therefore was chosen for all binding studies to maintain uniformity. Each PDZ sample for the peptide titrations was 0.5 mM. Peptide titrations were carried out by the addition of small aliquots of the concentrated stock peptide, which was prepared by dissolving the solid peptide in the same buffer as the PDZ domain. The pH of the stock solution was checked to ensure that it was the same as the PDZ sample.

KirNC was prepared in 50 mM phosphate, pH 7.5, 50 mM NaCl, 2 mM DTT, and 1 mM EDTA. For all the KirNC complexes, separate samples of PDZ/KirNC at ratios of concentrations between 0.5 and 4 were prepared by premixing dilute samples of the stock proteins in the correct molar ratio and concentrating the samples to 300 μL using a Vivaspin concentrator (VivaScience AG) to give a final PDZ concentration of between 0.3 and 0.7 mM. Separate complex samples for each titration point were made using the same stock of proteins to minimize variations in sample conditions within a set of experiments. Furthermore, each set of titrations was done in duplicate. To ensure that complexes were formed, size-exclusion chromatography was carried out to isolate the complex from the unbound proteins, and SDS-PAGE gels were run to verify the presence of both proteins in the complex fraction. Furthermore, SDS gels were run before and after the NMR experiment to ensure that all proteins remained intact over the course of the NMR experiment.

NMR Spectroscopy. Spectra were recorded at 22 °C using a Bruker Avance 600 spectrometer fitted with a triple resonance, single *z*-axis gradient cryogenic probehead and a Varian Inova 800 MHz spectrometer equipped with a room-temperature triple resonance probehead. ^{1}H, ^{15}N, and ^{13}C assignments of the free and peptide-bound proteins were determined independently using the following experiments: ^{15}N-edited HSQC-NOESY (mixing time 150 ms), CBCA-(CO)NH, CBCANH, HBHA(CO)NH, HNCA, HN(CA)CO, HNCO, HN(CO)CA, and HNHA. Spectra were processed using the NMRPipe software package (*36*) and analyzed using NMRView5 (*37*) on a SGI-Irix workstation. Processing scripts were optimized for each experiment, but in general, each dataset was processed with a shifted sine-bell apodization function, and zero-filling was applied in all dimensions. Linear prediction was implemented to double the data size in the t_1 dimension to improve spectral resolution. Chemical shift indexing was performed using the CSI program (*38*). Unless otherwise specifically stated, all the spectra shown were obtained on the Bruker Avance 600 spectrometer.

Peptide Titration and Chemical Shift Mapping. In all data involving an analysis of a change of chemical shifts, a series of ^{15}N/^{1}H HSQC spectra was recorded. The weighted amide chemical shift differences δ between spectra 1 and 2 were calculated as $\delta = \sqrt{(\delta_1^{H}-\delta_2^{H})^2+((\delta_1^{N}-\delta_2^{N})0.17)^2}$, where δ^{H} and δ^{N} are the proton and nitrogen chemical shifts, respectively. Data were analyzed using NMRView, and the results were visualized using DASHA (*39*) or XMGrace. Dissociation constants for the PDZ-Kir2.1 peptide complexes were calculated from least-squares fitting of the change in chemical shifts as a function of ligand concentration to fit the binding isotherm $K_d = [P_f][L_f]/[PL]$, where P_f, L_f, and PL are the concentrations of the free protein, free ligand, and complex, respectively. Data were analyzed by GraphPad Prism V5.

Small-Angle X-ray Scattering (SAXS). Synchrotron SAXS data were collected at station 2.1 with a multiwire gas detector at the Daresbury SRS (*40*, *41*). Samples were measured at concentrations between 1 and 5 mg/mL covering a momentum transfer range of 0.01 Å^{-1} < q < 0.6 Å^{-1} with $q = 4\pi \sin \Theta/\lambda$ (where 2Θ is the scattering angle and λ is the X-ray wavelength of 1.54 Å). Samples were loaded into a temperature controlled (4 °C) brass cell containing a Teflon ring sandwiched by two mica windows, which defines a cell volume of 100 μL. Experimental data were collected in 60 s frames, and each frame was inspected for X-ray induced damage or aggregation. The background was deducted using the scattering from the cell filled with buffer. Data were processed with the programs OTOKO and GNOM to compute the radius of gyration (R_g) and maximum molecular dimension (D_{max}) by using standard procedures (*42*). Particle shapes at low resolution were reconstructed *ab initio* with the bead modeling program GASBOR (*43*), which represents the protein as a chain of dummy residues centered at the Cα-positions. An averaged and filtered representative (using DAMAVER) was calculated from 12 independent PDZ12 and 23 independent PDZ1−3 shape models (none of the PDZ12 and only one of the PDZ1−3 models were rejected in the averaging process). In addition, the program BUNCH (*44*) was applied to benefit from the known high-resolution PDZ domain structures and to explore the range of possible conformations due to the presence of flexible polypeptide segments linking and flanking those domains. The local meta-threading-server for protein structure prediction LOMETS (*45*) (http://zhang.bioinformatics.ku.edu/LOMETS) was used to generate atomic structures of the three PDZ domains of rat SAP97. All three domains were considered as easy targets using as best ranking templates the PDZ domain structures with PDB codes 2i1n, 2fne, and 1be9 for PDZ1, PDZ2, and PDZ3, respectively. Attached to PDZ3, a C-terminal helix followed by a β-strand was obtained in line with NMR results for this region (U4 linker segment). Rigid body modeling with these domains against scattering data was carried out as implemented in BUNCH. In the case of PDZ12, one of the two domains was kept fixed. The resulting PDZ12 model with the lowest goodness-of-fit value ($\chi = 3.6$) was used in subsequent BUNCH calculations for PDZ1−3, and its position was fixed (while PDZ3 and linker and terminal segments were allowed to move). Side chains in the linker and terminal regions were added with the program MAX-SPROUT (http://www.ebi.ac.uk/maxsprout).

RESULTS

Interdomain Interactions and Structure of the U3 and U4 Linker Region by NMR. All three single PDZ domains adopt folded conformations, as judged from the 2-D ^{1}H/^{15}N heteronuclear single quantum coherence (^{1}H/^{15}N HSQC) spectra. Complete backbone and near complete side chain ^{13}C/^{15}N/^{1}H NMR resonance assignments were obtained for the three single PDZ domains (PDZ1: aa 218−313; PDZ2: aa 314−406; and PDZ3 aa 473−546 flanked by the U3 (407−472) and U4 (547−577) linker regions) and the multiple domains (PDZ12: aa 218−406 and PDZ1−3: aa 218−577) (Figure 1) using standard triple resonance experiments. For the double and triple domains, ^{13}C/^{15}N/^{2}H samples were prepared. The resonances in the ^{1}H/^{15}N HSQC spectra of the single domain PDZ1 and 3 overlay very well with their corresponding resonances in the spectrum of the PDZ1−3 domains (Figure 2a); PDZ2 resonances show more variations when comparing the single and multiple domain spectra (Figure 2b,d vs c). The linewidths of the resonances in the single and multiple domain spectra are not significantly different. This contrasts the closely related protein, PSD-95, where significant line-broadening was observed in the spectra of PDS-95 PDZ12 when compared to the resonances in the single domains (*46*). A residue-by-residue comparison of chemical shifts of the 2-D ^{1}H/^{15}N HSQC resonances in the different domains shows that domain 2 is the one most affected (average shift changes of approximately 0.05 ppm) when covalently attached to either the U3 + PDZ3 + U4 segment or PDZ1 (Figure 3a,b), suggesting that PDZ2 is placed between PDZ1 and U3 + PDZ3 + U4. Further evidence that interdomain interactions are either very weak or absent comes from the lack of shift changes when saturating amounts of unlabeled PDZ1 are added to ^{15}N-labeled PDZ2. Finally, the transient nature of any interdomain interaction is supported by the presence of only very small reciprocal shift changes (<0.04 ppm) in PDZ1 or PDZ3 when linking PDZ2 to it. Linking PDZ1 or U3 + PDZ3 + U4 to PDZ2 commonly affects the resonances from H340−Y348 on PDZ2. These residues are located in the unstructured β2/β3 loop region (*9*) (Figure 3c).

To probe the domain−domain interactions and possible orientation, paramagnetic relaxation enhancements (PRE)

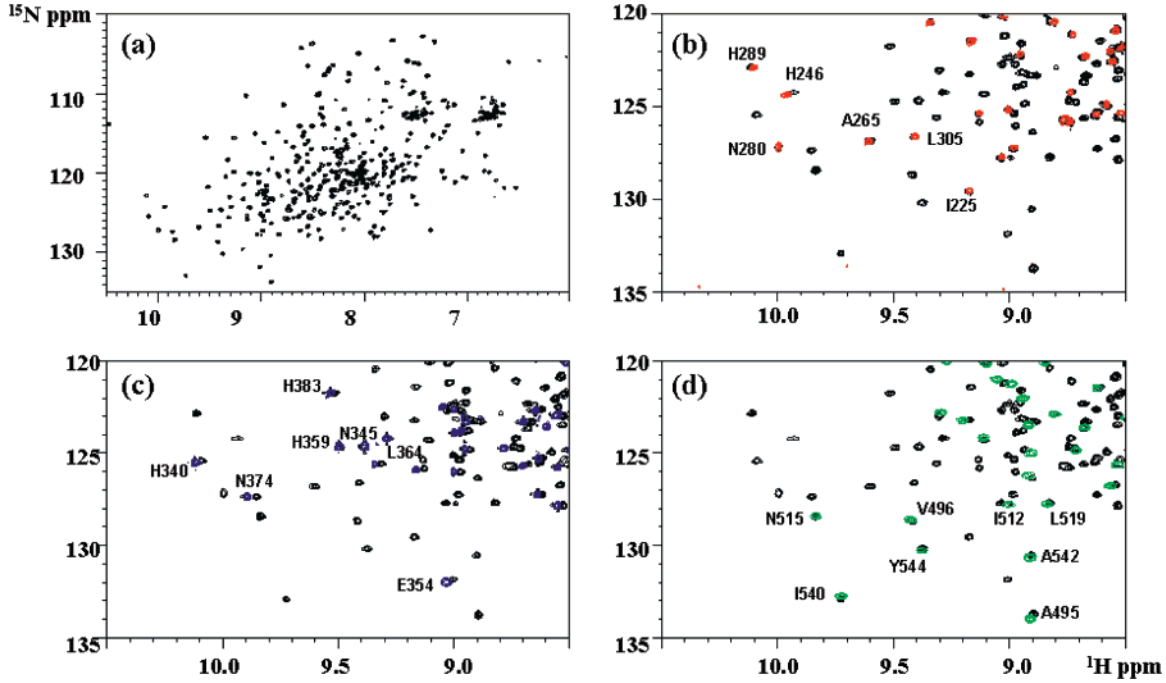

FIGURE 2: (a) ^{15}N/^{1}H HSQC spectrum of PDZ1−3. (b−d) Sections of an overlay of the HSQC spectra for (b) PDZ1 (aa 218−313, red) (c) PDZ2 (aa 314−406, blue), and (d) U3 + PDZ3 + U4 (aa 407−577, green) with the spectrum of full-length PDZ1−3 (black). Examples of assigned residues are shown. The systematic shifts observed are due to small variations in the pH of the samples.

were also used (*47*). A model of the structure of SAP97 suggested cysteine 377 in PDZ2 as a suitable site for attaching a paramagnetic probe to observe paramagnetic relaxation effects between the PDZ domains. A triple PDZ domain mutant (C275S) with the remaining cysteine residue at position 377 was modified with a nitroxide spin-labeled MTSL. Only limited PRE are observed, with complete line-broadening seen for resonance of residues in the immediate vicinity of the spin-labeled sites and residues A441, R461, H469, F489, and I511 in the U3 linker and PDZ3; measurable reduction in intensities of up to 50% were observed for residues D219-E224, K308, and A312 in PDZ1 (see Supporting Information Figure 1). We conclude at this stage that although interactions exist between PDZ2 and PDZ1/3, these are likely to be very weak and transient.

We report here the first experimental data revealing the structural characteristics of the U3 and U4 regions. Previous modeling studies have reported that the U3 region adopts a β-turn and that the U4 region consists of an α-helix (*41*). Chemical shift indices (CSI) of the assigned backbone and Cβ-resonances (Figure 4a) show secondary structure composition distribution that is in good agreement with the secondary structures obtained experimentally in the structures of SAP97 PDZ1 (*8*) and PDZ2 (*9*). Both CSI and Cα/Co chemical shift differences for the U3 linker region (residues 407−462) indicate an absence of stable secondary structure(s) since no more than three consecutive residues show shift differences that would define a β-strand or α-helical structure. On the other hand, the U4 linker region is a stable helix from residues 547−560 followed by a short β-strand 561−564 (Figure 4a).

Heteronuclear ^{15}N/^{1}H NOE (hNOE) data for PDZ1−3 show residues in distinct regions of the protein exhibiting different motions on the picosecond time scale; negative hNOE are confined to the N- and C-termini and the U3 linker region aa 407−462 (Figure 4b). The resonances from the short linker between PDZ1 and PDZ2 have reduced hNOE, with average values of about 0.65, whereas the average hNOE for the U3 linker region is approximately zero (Figure 4b). Hence, we conclude that the U3 linker region has considerable mobility in addition to being largely unstructured.

SAP97 PDZ12 and PDZ1−3 Conformation using SAXS. We carried out SAXS studies on the double and triple domain. The analysis confirmed that both domain constructs are monomeric in solution and that their radii of gyration (R_g) and maximum dimensions (D_{max}) indicate elongated but still rather globular molecules. Preliminary results of this study have been reported recently (*48*). Figure 5 shows the processed X-ray scattering profiles and distance distribution functions $p(r)$. The latter demonstrates the contribution of individual and separated domains (manifest as shoulders on the $p(r)$ functions) to the overall scattering. As would be expected, the radius of gyration of PDZ12 is smaller than the one of PDZ1−3 (23.6 ± 0.1 Å vs 33.3 ± 0.1 Å); the data obtained gave maximum molecular dimensions for PDZ12 and PDZ1−3 to be 75 ± 3 and 115 ± 6 Å, respectively. Several independent *ab initio* low-resolution shape models were reconstructed with GASBOR (*43*). Their average consensus conformations are presented in Figure 6 as transparent surfaces. The shape of the double domain reveals a symmetrical molecule comprised of two distinct and apparently non-interacting domains, in broad agreement with the NMR data; the overall shape is similar to a dumbbell. On the other hand, the triple domain is elongated and non-symmetrical, comprised of two to three distinct components. If we consider that the double domain PDZ12 is 18 kDa, and the triple domain is 36 kDa, one would expect the linker region plus the third domain to comprise half the mass of the triple domain. The shape reconstruction of the scattering data, therefore, suggests an extended but still rather compact three-dimensional structure for the triple domain.

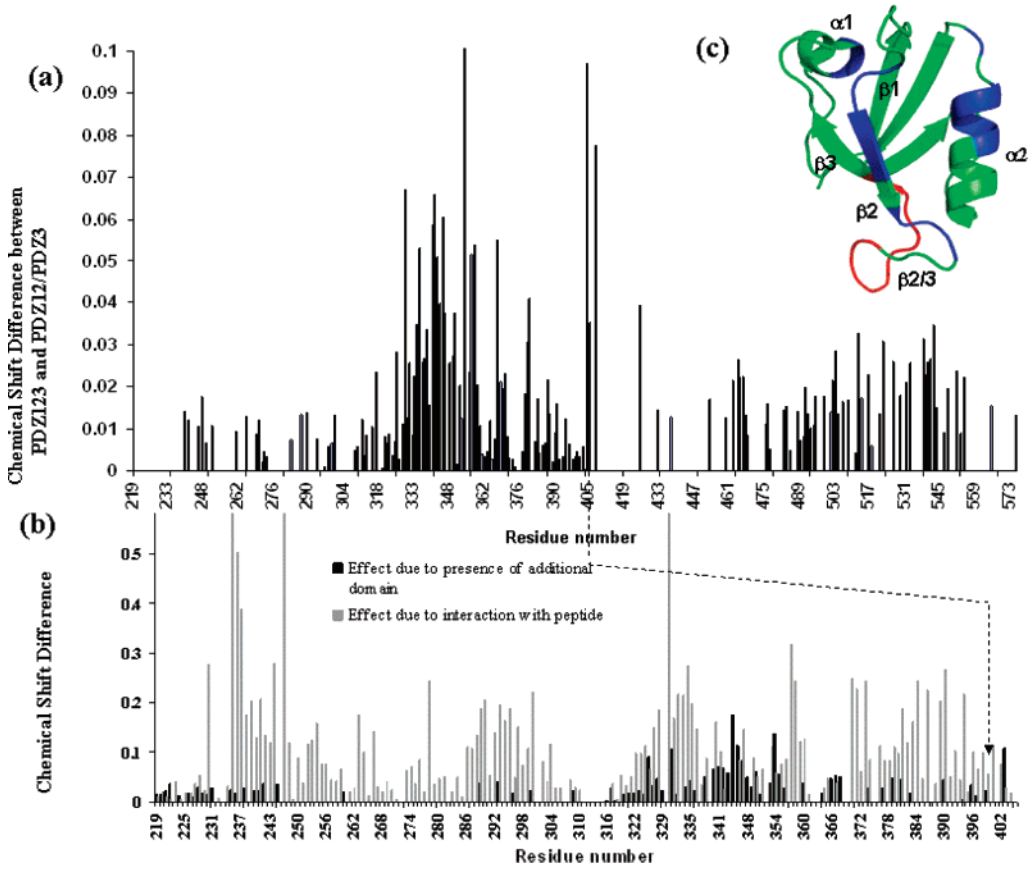

FIGURE 3: Histogram showing the shift differences measured as $\delta = \sqrt{(\delta_1^{H}-\delta_2^{H})^2+((\delta_1^{N}-\delta_2^{N})0.17)^2}$, where δ^H and δ^N are, respectively, the proton and nitrogen chemical shifts. In panel a, the shifts of PDZ12 and U3 + PDZ3 + U4 are compared with those of PDZ1−3. In panel b, the shifts of PDZ1 and PDZ2 are compared with those of PDZ12 (black). The shift changes induced upon binding Kir2.1 peptide ^{418}EPRPLRRESEI^{428} are shown in gray as a comparison to show the magnitude of shifts that can be expected when strong interactions occur. (c) Backbone cartoon of PDZ2 (ref *9*; PDB code 2g2l) with residues whose resonances significantly shift ($\delta \geq 0.3$ ppm) on binding. ^{418}EPRPLRRESEI^{428} are highlighted in blue, and residues affected by the presence of PDZ1 or U3 + PDZ3 + U4 ($\delta \geq 0.05$ ppm) are in red. The molecular graphics drawing program PYMOL (http://pymol.sourceforge.net) was used to produce this figure.

The shape averaging process revealed good agreement among individual shapes of PDZ12 characterized by a normalized spatial discrepancy (NSD) value of only 1.042 ± 0.021. In contrast, the individual shapes of PDZ1−3 produced a significantly larger NSD value (1.559 ± 0.226) on averaging, which indicates that its representative average shape is associated with larger variations. To assess further the likely conformational variations of these multidomain constructs, we carried out rigid body modeling (*44*), which also allows the exploration of possible conformations of the flexible connecting peptide segments (the NMR data described above support the mobile nature of the linker regions). The models for PDZ12 produced essentially three closely related locations for the second PDZ domain with respect to the first PDZ domain (see Figure 6a). In contrast, the models for PDZ1−3 displayed a variety of arrangements (see Figure 6b). Yet, essentially, PDZ3 is located at a distance of around 40 Å (center of mass distance between PDZ domains) at either side of the double domain PDZ12 (Figure 6b), whereby the linker U3 is not stretched out but sampling the conformational space in-between PDZ domains. Interestingly, in 25% of the models, PDZ3 is closer to PDZ1, which can be described as domain alignment PDZ2−PDZ1−PDZ3 as compared to the more frequent occurrence of PDZ1−PDZ2−PDZ3 during rigid body modeling.

In Vitro Characterization of the Interactions between SAP97 PDZ and Kir2.1 Cytoplasmic Domain by NMR. Complexes between Kir2.1 aa 1−76 fused to aa 189−428 (termed KirNC) and ^{15}N/^{2}H PDZ samples as single and multiple domains were prepared. For each of the complexes, a series of ^{15}N/^{1}H TROSY spectra of PDZ with increasing KirNC/PDZ ratios show decreasing overall signal-to-noise ratios (Figures 7 and 8). Figures 7 and 8b show the data for the complexes obtained using the two isolated single domains, PDZ1 and PDZ2. Figure 8a shows the data for PDZ1−3. Similar line-broadening effects were observed for the complex between PSD-95PDZ12 and KirNC (*30*).

Both domain- and residue-specific chemical shift changes and line-broadening are present, implying that the effects are due to specific interactions rather than nonspecific aggregation; the decrease in intensities at higher concentrations of KirNC results from the presence of a higher mole fraction of the large complex.

The degree of line-broadening, as a function of the amount of KirNC present, is greatest for PDZ2 and least for PDZ3, regardless of whether single or multiple domain proteins are used (Figure 8b vs c). Whereas many resonances from PDZ2 are completely broadened, resonances from the corresponding residues in PDZ1 and PDZ3 are still observed, with the PDZ3 resonances being generally more intense than those from PDZ1.

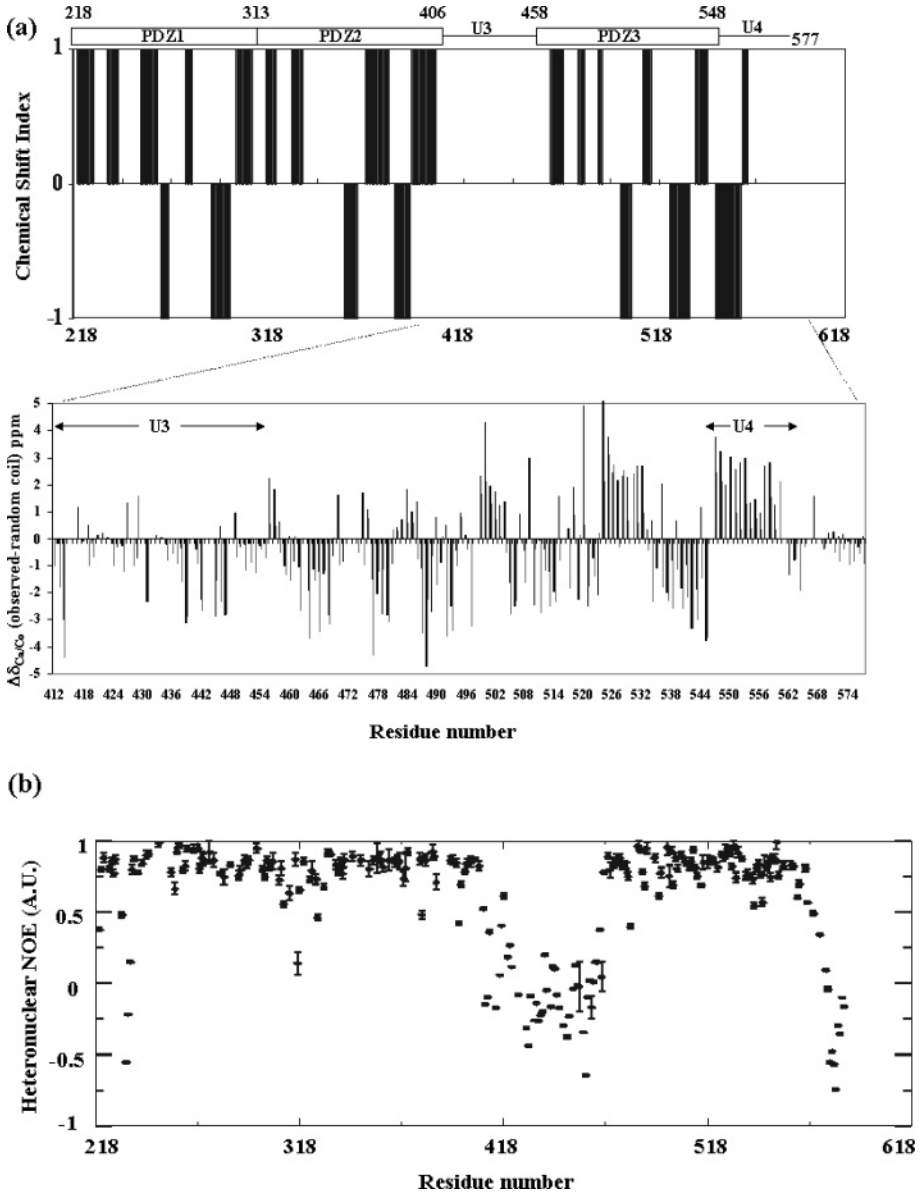

FIGURE 4: (a) Top: consensus chemical shift indexes for SAP97 PDZ1−3 based on an analysis of Cα, Cβ, CO, and Hα chemical shifts for each residue, with bars above the central line for β-structure and below the line for α-structure. Bottom: ^{13}Cα (black) and ^{13}Co (gray) secondary chemical shifts for U3 + PDZ3 + U4 calculated using random coil reference values from ref *38*. (b) Heteronuclear ^{15}N/^{1}H NOEs measured for ^{15}N/^{1}H PDZ1−3.

It is difficult to obtain reliable and precise affinity constants for the interactions between KirNC and the PDZ domains of SAP97 because of the complexity of the system (e.g., a tetrameric KirNC binding to SAP97 that potentially has three available binding sites). To simplify the problem, we used the peptide ligand ^{418}EPRPLRRESEI^{428}, which contains the consensus PDZ-binding motif to obtain the relative affinities of the three individual PDZ domains for KirNC. The K_d values estimated from fluorescence anisotropy data (at 50 mM NaCl) for the isolated PDZ2 and PDZ1 are, respectively, 76 ± 2 and 197 ± 7 μM. The binding of the peptide to PDZ3 is too weak for detection by fluorescence anisotropy. Fluorescence experiments performed using the multiple domains PDZ12 and PDZ1−3 yield apparent K_d values of, respectively, 38 ± 1.5 and 42 ± 1.2 μM (see Supporting Information Figure 2a). These values most likely reflect interactions with the major binding site, which is PDZ2 in both cases. Notably, the presence of an extra U3 + PDZ3 domain in PDZ1−3 does not appear to have a significant effect on the affinity of PDZ12 for the peptide.

Analyses of the peptide-dependent NMR chemical shifts using single and triple PDZ domains give similar results. Figure 9a shows the binding isotherms for ^{418}EPRPLRRESEI^{428} using the isolated PDZ2 domain (black) and PDZ2 within PDZ1−3 (red). The two sets of normalized binding curves are almost indistinguishable. The presence of the extra domains does not affect the affinity of PDZ2 for the peptide. PDZ1 shows similar results (see Supporting Information Figure 2b). The lack of saturation of the PDZ3 NMR chemical shift changes (Figure 9b) with increasing concentrations of peptide provides evidence that PDZ3 binds much more weakly than the other two domains.

Therefore, there appears to be a good correlation between the extent of KirNC-induced line-broadening in the PDZ resonances and the peptide-binding affinities; the higher the affinity, the more widespread the line-broadening effects. In

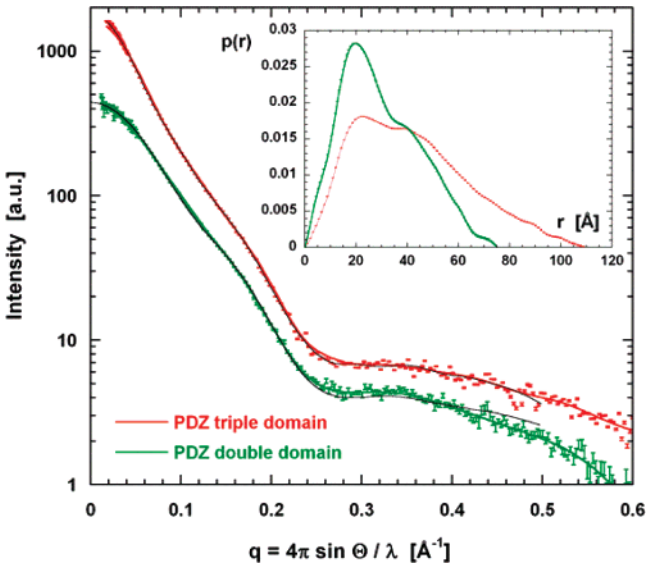

FIGURE 5: SAXS intensities of PDZ12 (green) and PDZ1−3 (red) as a function of momentum transfer are shown together with their respective X-ray distance distribution functions (inset). Dots with error bars represent experimental data; green and red lines are fits from the ab initio models for PDZ12 and PDZ1−3, respectively; and black lines correspond to fits from rigid body models.

the intact multiple domain protein, therefore, PDZ2 is the strongest binder, and the third domain is the weakest to KirNC.

The chemical shifts of the resonances from the U3 region remain largely unperturbed and intense (Figure 8c). This further suggests that the chemical environment of U3 is essentially unaffected by the bound KirNC. It is, therefore, unlikely that U3 has to move out of the way for KirNC to bind to PDZ2.

DISCUSSION

It has not been possible to crystallize PDZ1−3 (*9*). Neither has the structure of full-length SAP97 been determined at atomic resolution. The NMR and SAXS data presented here provide the first conformational analyses of the three SAP97 PDZ domains studied as intact multiple domains. Both structural methods show that in the triple PDZ protein, each SAP97 PDZ folds up as an independent domain with little short-range contacts between each other. Furthermore, both methods provide evidence to support the notion that PDZ1−3 adopts a range of preferred conformations. The NMR data show that the large U3 linker region does not have stable secondary structures, while the U4 linker has a $\alpha\beta$-structure. Both the U3 and the U4 linker regions have a higher mobility than the folded domains.

The SAXS data are consistent with the U3-PDZ3 domain able to take up different positions with respect to the PDZ12 subunit. At the same time, the overall size parameters (R_g and D_{max}) of the triple domain show that the PDZ3 domain is not completely disconnected and distant from the first two domains but is still within a 40 Å distance from one of these

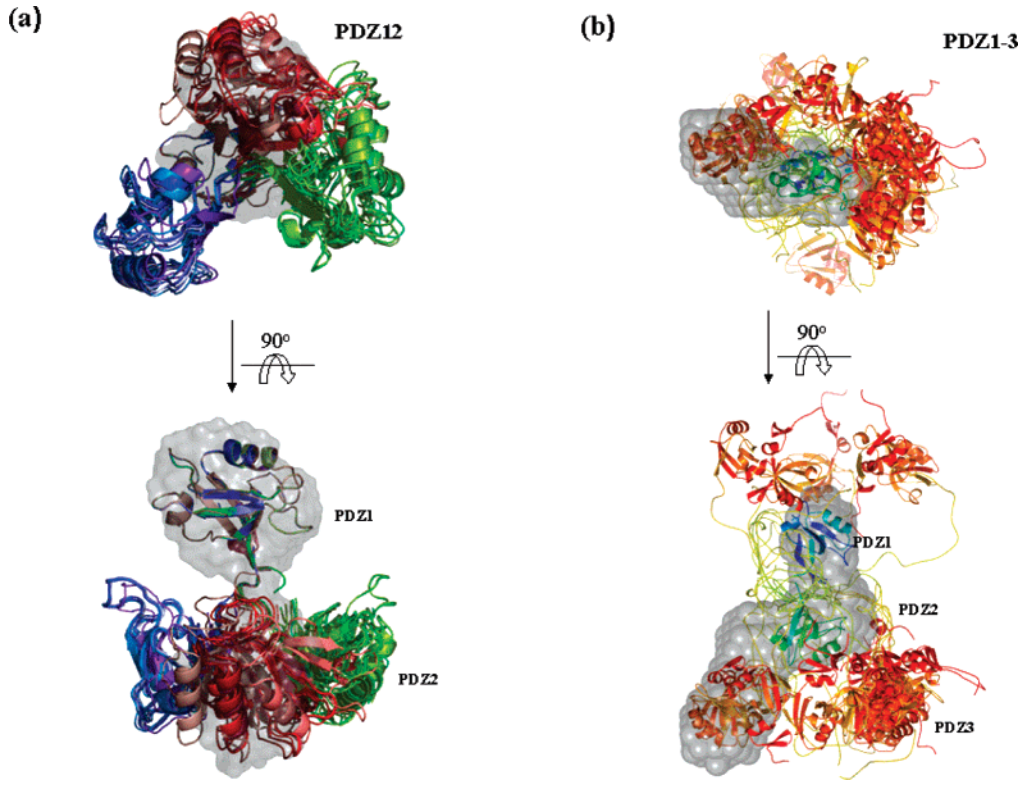

FIGURE 6: Conformational variation of structural models for (a) PDZ12 (aa 218−406) and (b) PDZ1−3 (aa 218−577) from SAXS data shown in two perpendicular orientations. The average ab initio low-resolution shape models are represented by their surface envelope in a transparent light gray color. Twenty rigid body models for the double and triple PDZ domain calculated with BUNCH are depicted as ribbon models. In the case of PDZ12, all models were superimposed on PDZ1, revealing three closely related positions for PDZ2 (highlighted in red, blue, and green). The group of red models was used to overlay the consensus shape calculated ab initio. The rigid body models for PDZ1−3 are in rainbow colors, which results in blue for PDZ1, green for PDZ2, and red/orange for PDZ3 including the C-terminal U4 segment. This color scheme highlights the U3 linker segment in yellow. All models were superimposed on their PDZ12 domains, exposing the conformational variety of PDZ1−3 domain arrangements. The molecular graphics drawing program PYMOL (http://pymol.sourceforge.net) was used to produce this figure.

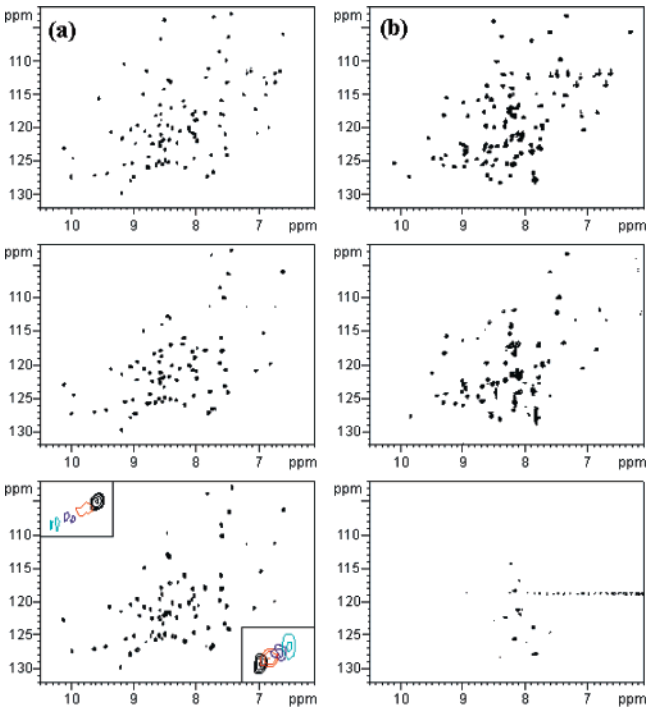

FIGURE 7: $^{15}N/^{1}H$ TROSY spectra showing (a) PDZ1 in the presence of increasing amounts of KirNC. Concentration ratios of PDZ to KirNC are 1:0 (top), 1:0.5 (middle), and 1:4 (bottom). Insets show changes in both chemical shifts and linewidths of two selected resonances. This demonstrates the formation of complexes; if the line-broadening is due to nonspecific interactions/aggregation, it is likely that only progressive line-broadening is observed. (b) PDZ2 in the presence of increasing amounts of KirNC. Concentration ratios of PDZ to KirNC are 1:0 (top), 1:0.5 (middle), and 1:3 (bottom).

domains. The SAXS data imply that there is a certain degree of compactness in the SAP97 aa 218−577. This is supported by NMR paramagnetic relaxation enhancement data, which show that a very small region of PDZ3 is within distance ranges to experience some line-broadening effects from the nitroxide spin label in position C377 of PDZ2. It is surprising that PDZ3 it is not sampling a much larger conformational space given the significant mobility and lack of stable secondary structure in U3. It is tempting to suggest that the U3 linker tethers PDZ3 to PDZ2, enabling interactions of PDZ3 with PDZ2 to form transiently. This tethering helps to bring the PDZ domains closer together, making it possible for SAP97 to function as a scaffold whereby the PDZ domains interact simultaneously with a variety of protein partners to form large productive complexes. At the same time, the mobility of U3 ensures that this linker is unlikely to block access to PDZ2 as had been previously proposed (*15*). This is particularly pertinent for the interactions involving large proteins such as cytoplasmic domains of the potassium inward rectifiers. There had been suggestions that the binding of target proteins to PDZ2 and U3 might be mutually exclusive, requiring a conformational displacement of U3 in order that several target proteins can bind simultaneously. However, the retained mobility, the lack of chemical shift perturbation of U3 resonances when SAP97 is bound to KirNC, and the fact that U3 + PDZ3 does not influence the binding affinity of PDZ2 to Kir2.1 all suggest two things. First, the U3 region does not block access to the PDZ2 ligand-binding site and, second, U3 is free to bind to other proteins, such as caveolin-3, to form ternary complexes (*34*).

We recognize that the 218−577 region of SAP97 studied here is only a portion of a larger protein. However, it is interesting to note that full-length SAP97 adopts a mixture of conformations, with 65% appearing as extended rod-like monomeric particles and the remaining 35% as C-shaped/ring-like structures as reported (*14*). Furthermore, using biochemical and modeling approaches, the N- and C-terminal regions of SAP97 appear to come close together to give SAP97 its U-shaped conformation (*15*). Hence, the restricted conformational dynamics found here for the PDZ region concurs with the previous results. It may well be that this region acts like a pivot around which the N- and C-terminal regions move, with the U3 linker additionally acting as a restraining tether.

Here, we additionally address the question as to whether binding to the peptides adequately represents interactions with large target proteins. The addition of the Kir2.1 peptide and cytoplasmic domain both cause specific perturbations to the NMR resonances of the same residues in each of the PDZ domains; all these residues either make up the putative ligand-binding groove or are in close proximity to this site.

Analysis of the titration of KirNC into SAP 97 on a residue-by-residue basis provides details of similarities and differences in the interaction of Kir2.1 with SAP97 PDZ domains. For example, the resonance of L390 in PDZ2 is one of the first to completely broaden when either Kir2.1 peptide and KirNC is present; on the other hand, the equivalent residue, L296, in PDZ1 is not affected at all when either ligand is present. Furthermore, in the NMR structure of SAP97 PDZ1-NR2B (*8*), peptide complex residues G235, F236, S237, I238, A239, V293, L296, and K297 have close contacts with residues from the peptide. In the PDZ2-GluR-A peptide complex (*9*), similar hydrophobic and electrostatic contacts are present. In SAP97 PDZ1 and PDZ2, these residues are conserved, whereas in PDZ3, S237 and V293 (in PDZ1) are replaced, respectively, by N478 and A528. Resonances from both S237 and V293 in PDZ1 and the corresponding S331 and V387 in PDZ2 are among the ones most affected (shift and line-broadening) upon Kir2.1 binding; yet the resonance from N478 in PDZ3 is only slightly broadened even when a 1:4 PDZ1−3/KirNC complex is formed. Therefore, it is likely that the variations in several key amino acids between PDZ1/PDZ2 and PDZ3, some of which are distal from the putative ligand-binding pocket and groove, are responsible for the domain-dependent differences in binding affinity for Kir2.1.

Experiments using other biophysical methods to obtain quantitative binding constants of the individual domains in the intact PDZ1−3 protein are non-trivial. This is due to the difficulties in deconvoluting the affinities of the individual domains in the intact protein; the data here at least provide a quantitative indication of the relative binding affinities of each domain in the intact multiple PDZ protein. Since the resonances from all three PDZ domains of SAP97 are affected when KirNC is present, it is likely that a complicated mixture of complexes may be present in solution. For example, one species could be a tetrameric assembly of KirNC interacting with all three domains of one molecule of PDZ1−3 and with only PDZ2 of another molecule. Another species might be tetrameric KirNC interacting with

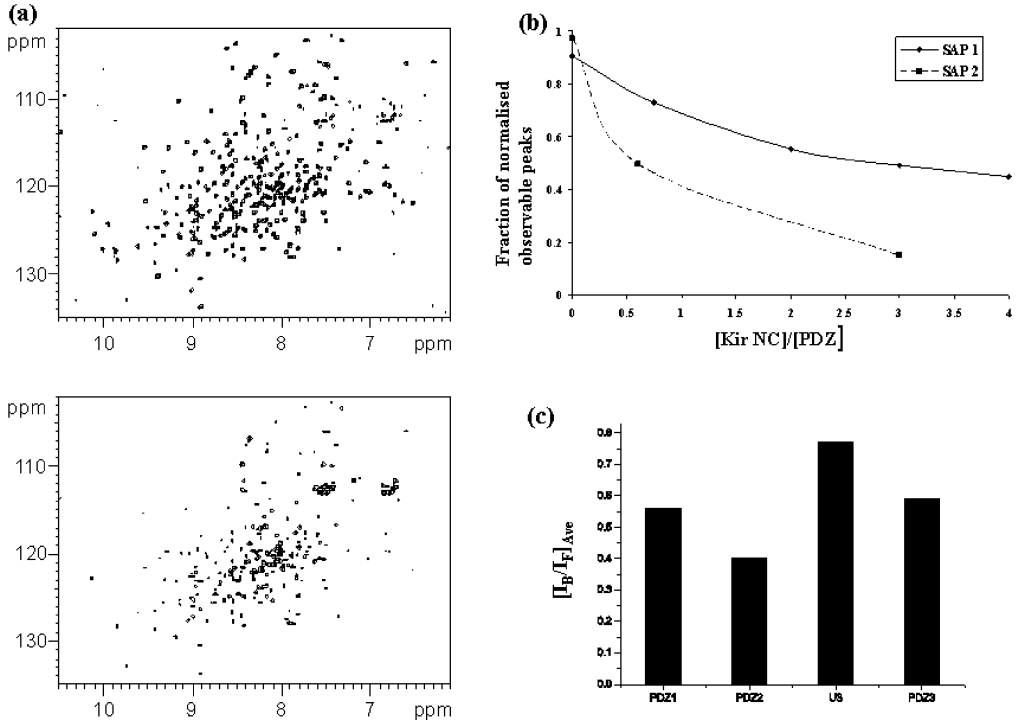

FIGURE 8: SAP97 PDZ interactions with KirNC. (a) PDZ1−3 in the presence of increasing amounts of KirNC. Concentration ratios of PDZ12 to KirNC are 1:0 (top) and 1:4 (bottom). Many resonances from domains 1 and 3 of PDZ1−3 remain detectable in the presence of excess KirNC. (b) Comparison of the fraction of NMR resonances observed for PDZ1 and PDZ2 upon addition of increasing concentrations of KirNC. At each concentration of KirNC, the resonance intensities are normalized to the most intense and unaffected resonance from the individual C-terminus residue of the PDZ domain. (c) Comparison of the fraction of resonances observed in a sample containing a 4-fold excess (monomer concentrations) of PDZ1−3 to Kir2.1. The resonances from PDZ1, PDZ2, U3, and PDZ3 are all affected but to different extents, with PDZ2 the most and U3 the least affected.

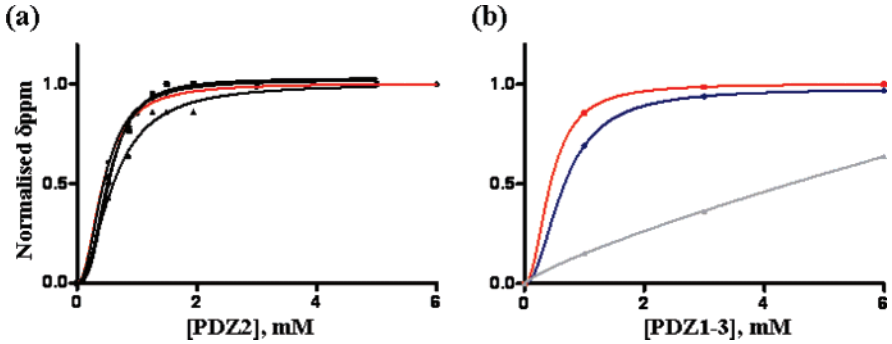

FIGURE 9: NMR binding curves for the interaction of KirNC peptide ^{418}EPRPLRRESEI^{428} with (a) isolated PDZ2 (0.4 mM) and (b) PDZ1−3 (0.5 mM), with the averaged shift changes colored differently for each of the three domains (PDZ1 (blue), PDZ2 (red), and PDZ3 (black)). The red curve in panel a is the same curve as shown in panel b. The data were analyzed by GraphPad Prism 5 software using a nonlinear least-squares fit for a one-site binding model. The shift changes $\delta = \sqrt{(\delta_1^H-\delta_2^H)^2+((\delta_1^N-\delta_2^N)0.17)^2}$ for specific resonances are normalized and plotted as a function of peptide concentration. For PDZ1−3, the solid lines in the titration of domains 1 and 2 represent the best fit of the experimental data to the equilibrium equation describing binding to a single ligand site. In the case of PDZ3, an estimated association constant was used to simulate a titration curve.

two molecules of SAP97 via domains 1 and 2 simultaneously. A third species could take the form of each subunit of the KirNC tetramer interacting with only PDZ2 of four separate PDZ1−3 molecules. Preliminary data show that the major stable form isolated by size-exclusion chromatography has a molecule mass of about 260 kD, suggesting the third species to be the likely predominant form. In this study, the binding affinities of KirNC to single and multiple SAP97 PDZ domains are not significantly different, suggesting that interdomain cooperativity between the different SAP97 PDZ domains for interactions with KirNC is unlikely.

In summary, we have shown that the U3 and U4 regions of SAP97 are mobile, with U3 largely unstructured and U4 containing a helix followed by a short β-strand. The SAP97 triple PDZ domain protein adopts an extended conformation with restricted dynamics. Each domain is able to bind KirNC and with an affinity that mirrors those observed for the peptide ($K_d^{EPRPLRRESEI}$: PDZ2 < PDZ1 < PDZ3). It is, therefore, most likely that specific amino acids determine the higher affinity for the second PDZ domain rather than this domain being more conformationally favored than the other two to interact with the large cytoplasmic domain of Kir2.1. The preferential binding to the second domain means that, *in vivo*, a 1:1 stoichiometry predominates (i.e., one Kir2.1 tetramer binds, via its C-terminal domain, to four SAP97 at the second PDZ domain). The remaining PDZ1

and PDZ3 are, consequently, free to bind other proteins that have higher relative affinities for these domains. The restricted dynamics of PDZ1−3 is postulated to have a role in positioning the simultaneously binding proteins in sufficiently close proximity to form productive complexes.

ACKNOWLEDGMENT

The expert advice and useful discussions with Dr. Alexander Golovanov of the University of Manchester are acknowledged. Dr. Geoff Kelly of the U.K. National Institute for Medical Research 800 MHz Facility at Mill Hill is gratefully acknowledged for his help.

SUPPORTING INFORMATION AVAILABLE

Two figures as described in the text. This material is available free of charge via the Internet at http://pubs.acs.org.

REFERENCES

1. Lahey, T., Gorczyca, M., Jia, X. X., and Budnik, V. (1994) The Drosophila tumor suppressor gene Dlg is required for normal synaptic bouton structure, *Neuron 13*, 823−835.
2. Mitic, L. L., and Anderson, J. M. (1998) Molecular architecture of tight junction, *Annu. Rev. Physiol. 60*, 121−142.
3. Rafael, J. A., Hutchinson, T. L., Lumeng, C. N., Marfatia, S. M., Chishti, A. H., and Chamberlain, J. S. (1998) Localization of Dlg at the mammalian neuromuscular junction, *Neuroreport 9*, 2121−2125.
4. Boekers, T. M. (2006) The postsynaptic density, *Cell Tissue Res. 326*, 409−422.
5. Muller, B. M., Kistner, U., Veh, R. W., Cases-Langhoff, C., Becker, B., Gungelfinger, E. D., and Garner, C. C. (1995) Molecular characterization and spatial distribution of SAP97, a novel presynaptic protein homologous to SAP90 and the Drosophila discs-large tumor suppressor protein, *J. Neurosci. 15*, 2354−2366.
6. Hata, Y., Nakanishi, H., and Takai, Y. (1998) Synaptic PDZ domain-containing protein, *Neurosci. Res. 32*, 1−7.
7. Feng, W., Long, J. F., Fan, J. S., Suetake, T., and Zhang, M. (2004) The tetrameric L27 domain complex as an organizational platform for supramolecular assemblies, *Nat. Struct. Mol. Biol. 11*, 475−480.
8. Wang, L., Piserchio, A., and Mierke, D. F. (2005) Structural characterization of the intermolecular interactions of synapse-associated protein-97 with the NR2B subunit of *N*-methyl-D-aspartate receptors, *J. Biol. Chem. 280*, 26992−26996.
9. von Ossowski, I., Oksanen, E., von Ossowski, L., Cai, C., Sundberg, M., Goldman, A., and Keinänen, K. (2006) Crystal structure of the second PDZ domain of SAP97 in complex with a GluR-A C-terminal peptide, *FEBS J.* 273, 5219−5229.
10. Cabral, J. H. M., Petosa, C., Sutcliffe, M. J., Raza, S., Byron, O., Poy, F., Marfatia, S. M., Chishti, A. H., and Liddington, R. C. (1996) Crystal structure of a PDZ domain, *Nature (London, U.K.) 382*, 649−652.
11. Zhang, Y., Dasgupta, J., Ma, R. L. Z., Banks, L., Thomas, M., and Chen, X. J. S. (2007) Structures of a human papillomavirus (HPV) E6 polypeptide bound to MAGUK proteins: Mechanisms of targeting tumor suppressors by a high-risk HPV oncoprotein, *J. Virol. 81*, 3618−3626.
12. McGee, A. W., Dakoji, S. R., Olsen, O., Bredt, D. S., Lim, W. A., and Prehoda K. A. (2001) Structure of the SH3-guanylate kinase module from PSD-95 suggests a mechanism for regulated assembly of MAGUK scaffolding proteins, *Mol. Cell 8*, 1291−1301.
13. Tavares, G. A., Panepucci, E. H., and Brunger, A. T. (2001) Structural characterization of the intramolecular interaction between SH3 and guanylate kinase domains of PSD-95, *Mol. Cell 8*, 1313−1325.
14. Nakagawa, T., Futai, K., Okamota, K., Walz, T., Hayashi, Y., and Sheng, M. (2004) Quaternary structure, protein dynamics, and synaptic function of SAP97 controlled by L27 domain interactions, *Neuron 44*, 453−467.
15. Wu, H. J., Reissner, C., Kuhlendahl, S., Coblentz, B., Reuver, S., Kindler, S., Gundelfinger, E. D., and Garner, C. C. (2000) Intramolecular interactions regulate SAP97 binding to GKAP, *EMBO J. 19*, 5740−5751.
16. Qian, Y., and Prehoda, K. E. (2006) Interdomain interactions in the tumor suppressor discs large regulate binding to the synaptic protein GukHolder, *J. Biol. Chem. 281*, 35757−35763.
17. Stanfield, P. R., Nakajima, S., and Nakajima, Y. (2002) Constitutively active and G-protein coupled inward rectifier K+ channels: Kir2.0 and Kir3.0, *Rev. Physiol. Biochem. Pharmacol. 145*, 47−179.
18. Nichols, C. G., and Lopatin, A. N. (1997) Inward rectifier potassium channels, *Annu. Rev. Physiol. 59*, 171−191.
19. Isomoto, S., Kondo, C., and Kurachi, Y. (1997) Inwardly rectifying potassium channels: Their molecular heterogeneity and function, *Jpn. J. Physiol. 47*, 11−39.
20. Cohen, N. A., Brenman, J. E., Snyder, S. H., and Bredt, D. S. (1996) Binding of the inward rectifier K+ channel Kir2.3 to PSD-95 is regulated by protein kinase A phosphorylation, *Neuron 17*, 759−767.
21. Nehring, R. B., Wischmeyer, E., Doring, F., Veh, R. W., Sheng, M., and Karschin, A. (2000) Neuronal inwardly rectifying K+ channels differentially couple to PDZ proteins of the PSD-95/SAP90 family, *J. Neurosci. 20*, 156−162.
22. Olsen, O., Liu, H., Wade, J. B., Merot, J., and Welling, P. A. (2002) Basolateral membrane expression of the Kir2.3 channel is coordinated by PDZ interaction with Lin-7/CASK complex, *Am. J. Physiol. Cell Physiol. 282*, 183−195.
23. Inanobe, A., Fujita, A., Ito, M., Tomoike, H., Inageda, K., and Kurachi, Y. (2002) Inward Rectifier K+ Channel Kir2.3 is localized at the postsynaptic membrane of excitatory synapses, *Am. J. Physiol. Cell Physiol. 282*, 1396−1403.
24. Leonoudakis, D., Mailliard, W. S., Wingerd, K. L., Clegg, D. O., and Vandenberg, C. A. (2001) Inward rectifier potassium channel Kir2.2 is associated with synapse-associated protein SAP97, *J. Cell Sci. 114*, 987−998.
25. Leonoudakis, D., Conti, L. R., Anderson, S., Radeke, C. M., McGuire, L. M. M., Adams, M. E., Froehner, S. C., Yates, J. R., and Vandenberg, C. A. (2004) Protein trafficking and anchoring complexes revealed by proteomic analysis of inward rectifier potassium channel (Kir2.x)-associated proteins, *J. Biol. Chem. 279*, 22331−22346.
26. Leonoudakis, D., Conti, L. R., Radeke, C. M., McGuire, L. M. M., and Vandenberg, C. A. (2004) A multiprotein trafficking complex composed of SAP97, CASK, Veli, and Mint1 is associated with inward rectifier Kir2 potassium channels, *J. Biol. Chem. 279*, 19051−19063.
27. Nishida, M., and MacKinnon, R. (2002) Structural basis of inward rectification: Cytoplasmic pore of the G protein-gated inward rectifier GIRK1 at 1.8 Å resolution, *Cell 111*, 957−965.
28. Kuo, A. L., Gulbis, J. M., Antcliff, J. F., Rahman, T., Lowe, E. D., Zimmer, J., Cuthbertson, J., Ashcroft, F. M., Ezaki, T., and Doyle, D. A. (2003) Crystal structure of the potassium channel KirBac1.1 in the closed state, *Science (Washington, DC, U.S.) 300*, 1922−1926.
29. Pegan, S., Arrabit, C., Zhou, W., Kwiatkowski, W., Collins, A., Slesinger, P. A., and Choe, S. (2005) Cytoplasmic domain structures of Kir2.1 and Kir3.1 show sites for modulating gating and rectification, *Nat. Neurosci. 8*, 279−287.
30. Pegan, S., Tan, J., Huang, A., Slesinger, P. A., Riek, R., and Choe, S. (2007) NMR studies of interactions between C-terminal tail of Kir2.1 channel and PDZ12 domains of PSD-95, *Biochemistry 46*, 5315−5322.
31. Gardoni, F., Mauceri, D., Fiorentini, C., Bellone, C., Missale, C., Cattabeni, F., and Di Luca, M. (2002) CaMKII-dependent phosphorylation regulates SAP97/NR2A interaction, *J. Biol. Chem. 45*, 44745−44752.
32. Peiretti, F., Deprez-Beauclair, P., Bonardo, B., Aubert, H., Juhan-Vague, I., and Nalbone, G. (2003) Identification of SAP97 as an intracellular binding partner of TACE, *J. Cell. Sci. 116*, 1949−1957.
33. Sabio, G., Arthur, J. S. C., Kuma, Y., Peggie, M., Carr, J., Murray-Tait, V., Centeno, F., Goedert, M., Morrice, N. A., and Cuenda, A. (2005) p38γ regulates the localization of SAP97 in the cytoskeleton by modulating its interaction with GKAP, *EMBO J. 24*, 1134−1145.
34. Folco, E. J., Liu, G. X., and Koren, G. (2004) Caveolin-3 and SAP97 form a scaffolding protein complex that regulates the

voltage-gated potassium channel Kv1.5, *Am. J. Physiol.: Heart Circ. Physiol. 287*, 681−690.
35. Lee, S. S., Weiss, R. S., and Javier, R. T. (1997) Binding of human virus oncoproteins to hDlgySAP97, a mammalian homologue of the Drosophila discs large tumor suppressor protein, *Proc. Natl. Acad. Sci. U.S.A. 94*, 6670−6675.
36. Delaglio, F., Grzesiek, S., Vuister, G. W., Zhu, G., Pfeifer, J., and Bax, A. (1995) Nmrpipe: A multidimensional spectral processing system based on unix pipes, *J. Biomol. NMR 6*, 277−293.
37. Johnson, B. A., and Blevins, R. A. (1994) NMR View: A computer program for the visualization and analysis of NMR data, *J. Biomol. NMR 4*, 603−614.
38. Wishart, D. S., and Sykes, B. D. (1994) The C-13 chemical shift index: A simple method for the identification of protein secondary structure using C-13 chemical shift data, *J. Biomol. NMR 4*, 171−180.
39. Orekhov, V. Y., Nolde, D. E., Golovanov, A. P., Korzhnev, D. M., and Arseniev, A. S. (1995) Processing of heteronuclear NMR relaxation data with the new software DASHA, *Appl. Magn. Reson. 9*, 581−588.
40. Towns-Andrews, E., Berry, A., Bordas, J., Mant, P. K., Murray, K., Roberts, K., Sumner, I., Worgan, J. S., and Lewis, R. (1989) Time-resolved X-ray diffraction station: X-ray optics, detectors, and data acquisition, *Rev. Sci. Instrum. 60*, 2346−2349.
41. Lewis, R. (1994) Multiwire gas proportional counters: Decrepit antiques or classic performers, *J. Synchrotron Radiat. 1*, 43−53.
42. Grossmann, J. G., Hall, J. F., Kanbi, L. D., and Hasnain, S. S. (2002) The N-terminal extension of rusticyanin is not responsible for its acid stability, *Biochemistry 41*, 3613−3619.
43. Svergun, D. I., Petoukhov, M. V., and Koch, M. H. J. (2001) Restoring low-resolution structure of biological macromolecules from solution scattering using simulated annealing, *Biophys. J. 80*, 2946−2953.
44. Petoukhov, M. V., and Svergun, D. I. (2005) Global rigid body modeling of macromolecular complexes against small-angle scattering data, *Biophys. J. 89*, 1237−1250.
45. Wu, S., and Zhang, Y. (2007) LOMETS: A local meta-threading-server for protein structure prediction, *Nucleic Acids Res. 35*, 3375−3382.
46. Long, J. F., Tochio, H., Wang, P., Fan, J. S., Sala, C., Niethammer, M., Sheng, M., and Zhang, M. (2003) Supramodular structure and synergistic target binding of the N-terminal tandem PDZ domains of PSD-95, *J. Mol. Biol. 327*, 203−214.
47. Battiste, J. L., and Wagner, G. (2000) Utilization of site-directed spin labeling and high-resolution heteronuclear nuclear magnetic resonance for global fold determination of large proteins with limited nuclear Overhauser effect data, *Biochemistry 39*, 5355−5365.
48. Grossmann, J. G. (2007) Biological solution scattering: Recent achievements and future challenges, *J. Appl. Crystallogr. 40*, 217−222.

BI701257Z